Theoretical Fe-57 Mossbauer spectroscopy: isomer shifts of [Fe]- hydrogenase intermediates

Hedegard, Erik Donovan; Knecht, Stefan; Ryde, Ulf; Kongsted, Jacob; Saue, Trond

Published in:
Physical Chemistry Chemical Physics

DOI:
10.1039/c3cp54393e

2014

Can ^{57}Fe Mössbauer isomer shifts be calculated accurately without fitting? Isomer shifts for [Fe]-Hydrogenase Intermediates

Erik D. Hedegård,[*,†] Stefan Knecht,[‡] Jacob Kongsted,[†] Ulf Ryde,[¶] and Trond Saue[*,§]

Department of Physics, Chemistry and Pharmacy, University of Southern Denmark, Campusvej 55, Odense 5420 M, Denmark, Laboratory of Physical Chemistry, ETH Zürich, Wolfgang-Pauli-Straße 10, 8093 Zürich, Switzerland, Department of Theoretical Chemistry, Lund University, Chemical Centre, P.O. Box 124, S-221 00 Lund, Sweden, and Laboratoire de Physique Quantique (CNRS UMR 5626), IRSAMC, Université Paul Sabatier, 118 Route de Narbonne, F-31062 Toulouse cedex, France

E-mail: edh@sdu.dk; trond.saue@irsamc.ups-tlse.fr

[*]To whom correspondence should be addressed

[†]Department of Physics, Chemistry and Pharmacy, University of Southern Denmark, Campusvej 55, Odense 5420 M, Denmark

[‡]Laboratory of Physical Chemistry, ETH Zürich, Wolfgang-Pauli-Straße 10, 8093 Zürich, Switzerland

[¶]Department of Theoretical Chemistry, Lund University, Chemical Centre, P.O. Box 124, S-221 00 Lund, Sweden

[§]Laboratoire de Physique Quantique (CNRS UMR 5626), IRSAMC, Université Paul Sabatier, 118 Route de Narbonne, F-31062 Toulouse cedex, France

Abstract

Mössbauer spectroscopy is an indispensable technique and analytical tool in iron coordination chemistry. The linear correlation between the electron density at the nucleus ("contact density") and experimental isomer shifts has been used to link calculated contact densities to experimental isomer shifts. Here we have investigated for the first time relativistic methods of systematically increasing sophistication, including the eXact 2-Component (X2C) Hamiltonian and a finite-nucleus model, for the calculation of isomer shifts for iron compounds. While being of similar accuracy as the full four-component treatment, X2C calculations are far more efficient. We find that effects from spin orbit coupling can safely be neglected, leading to further speed up. Linear correlation plots using effective densities rather than contact densities versus experimental isomer shift leads to a correlation constant $a = -0.32\ a_0^{-3}$ mm s^{-1} (PBE functional) which is in close agreement to experimental findings. Isomer shifts of similar quality can thus be obtained both with and without fitting, which is not the case if one pursues *a priori* a non-relativistic model approach. As an application for a biologically relevant system, we have studied three recently proposed [Fe]-hydrogenase intermediates. The structures for these intermediates were extracted from QM/MM calculations using large QM regions surrounded by the full enzyme and a solvation shell of water molecules. We show that a comparison between calculated and experimentally observed isomer shifts can be used to discriminate between the different intermediates, whereas calculated atomic charges do not necessarily correlate with Mössbauer isomer shifts. Detailed analysis shows that the difference in isomer shifts between two intermediates is due to an overlap effect.

Introduction

It is needless to emphasize the role of coordination compounds with an iron metal center in inorganic and bio-inorganic chemistry. Apart from the obvious industrial interest in iron coordination compounds, the biological role played by iron is unmatched by any other metal. For instance, enzymes comprising heme units have been found in essentially all lineages of life. Another example are hydrogenase enzymes[2,3] which are promising candidates for hydrogen storage materials.

An important spectroscopic technique in iron chemistry is Mössbauer spectroscopy.[4] Although also applicable to other nuclei, its use to characterize iron compounds is by far dominating.[5,6] Mössbauer spectroscopy relies on the Mössbauer effect, which is the recoilless emission or absorption of γ radiation from a nucleus in a (solid) sample. A common source to create excited state iron nuclei is the radioactive ^{57}Co isotope, which decays by electron capture to the nuclear isomer $^{57\mathrm{m}}$Fe. The emitted γ-ray from the relaxation of the spin $I = 3/2$ to the nuclear ground $I = 1/2$ state of iron is then used to probe the sample (absorber).

Electrostatic interaction between electronic and nuclear charge distributions,

$$E^{e0} = \int \rho_e(\mathbf{r}_e)\phi_n(\mathbf{r}_n;R)d^3r_e; \quad \phi_n(\mathbf{r}_n;R) = \int \frac{\rho_e(\mathbf{r}_e)}{r_{en}} d^3r_n \tag{1}$$

notably its change upon nuclear excitation, may lead to a modification ΔE^{e0} of the nuclear γ-transition energy E_γ. The modification of the transition energy is in general different for source (s) and absorber (a) and gives rise to a non-zero isomer shift[7–9]

$$\delta = \frac{c}{E_\gamma}(\Delta E_a^{e0} - \Delta E_s^{e0}) \tag{2}$$

where c is the speed of light. The conversion factor of c/E_γ arises as the sample is brought to resonance by mechanically changing the relative motion of source and sample taking advantage of the Doppler effect. The isomer shift is accordingly given in units of speed, typically $\mathrm{mm\,s^{-1}}$. In older literature, the Mössbauer isomer shifts were often reported with respect to the source material in which ^{57}Co was embedded, whereas today it is more common to use a well-defined reference, which thereby takes the place of the source in the above expression. Typical examples of Mössbauer references are iron foil (α-Fe) and sodium nitroprusside $\mathrm{Na_2[Fe(NO)(CN)_5]\cdot 2\,H_2O}$.

The modulation of electrostatic interaction upon the change in nuclear size from ground to excited nuclear state can be expressed in terms of a first-order Taylor expansion[10,19] Neglecting

any dependence of the electronic charge density ρ_e on nuclear radial size then leads to

$$\Delta E^e = \left.\frac{\partial E^e}{\partial R}\right|_{R=R_0} \Delta R \approx \int \rho_e(\mathbf{r}_e) \left.\frac{\partial \phi_n(\mathbf{r}_e;R)}{\partial R}\right|_{R=R_0} \mathrm{d}^3 r_e \, \Delta R \tag{3}$$

where ΔR is change in the radial size parameter R between the excited and ground nuclear state. Since the derivative of the nuclear potential ϕ_n is an extremely local quantity one may formally extract an effective density $\bar{\rho}_e$, that is, the weighted average of the electron density over the finite-sized nucleus, from the integral:

$$\Delta E^e = \bar{\rho}_e \int \left.\frac{\partial \phi_n(\mathbf{r};R)}{\partial R}\right|_{R=R_0} \mathrm{d}^3 r \, \Delta R \tag{4}$$

This leads to the following expression for the Mössbauer isomer shift

$$\delta = \alpha(\bar{\rho}_e - \bar{\rho}_e^{\mathrm{ref}}), \tag{5}$$

where the isomer shift calibration constant

$$\alpha = -\left(\frac{4\pi Z c R_0^2}{5E_\gamma}\right)\frac{\Delta R_0}{R_0} \tag{6}$$

contains all constants and nuclear information. The effective density $\bar{\rho}_e$ is usually approximated by the contact density ρ_0, that is the density at the nuclear origin.

Quantum chemical calculations typically exploit the linear correlation

$$\delta = a(\bar{\rho}_e - C) + b. \tag{7}$$

between experimental isomer shifts and the contact shift[11–14] and using contact densities. This *ansatz* allows to absorb not only nuclear information, but also shortcomings of the chosen theoretical model chemistry into the fitting constants a and b (C is held constant in the fit), and so a is in general not equal to α. The first computational studies to make use fitting expressions such as

Eq. 7 were based on a relativistic but rather crude semi-empirical or Hartree-Fock methods.[11–13,15] Later, modern density functional theory with gradient corrected functionals were applied with success,[16–18] but without taking into account relativistic effects at all. While such an *ansatz* is efficient and fairly reliable it relies on error cancellations[14] and suffers from the fact that each new functional/method give a new correlation line (Eq. 7).

The most recent developments to ensure an appropriate account of relativistic effects were done by Filatov and co-workers who suggested a method that is independent of fitting.[19,20] In this model the isomer shift is calculated directly from 5 using a value of $\alpha = -0.31 \pm 0.04\ a_0^3$ mm s^{-1} from life-time measurements by Ladrière *et al.*[21] At the same time, it was also recommended to employ effective densities $\bar{\rho}$ which take into account the finite size of the nuclei. In order to include both relativity and sophisticated computational methods, Kurian and Filatov alternatively proposed[22] to scale non-relativistic effective densities obtained from DFT with a factor $\bar{\rho}_{\text{rel}}/\bar{\rho}_{\text{non-rel}}$ computed from CCSD(T) effective density calculations on atomic iron. The scaled densities were then used in Eq. 7 which led to results similar to quasi-relativistic ZORA calculations.[23,24]

The use of effective densities and the inclusion of relativity has also been considered by others and both effects have been shown to be of quantitative importance for heavier nuclei.[25,26] On the contrary, for iron both the role of relativity and the use of effective densities rather than contact densities remains less clear. An open question is thus to what extent relativistic effects should be included and whether spin-orbit coupling influences the isomer shift. Another unknown factor is how much a finite nucleus treatment will affect the isomer shift calculations. At present, it also remains to be established which of the two methods, Eq. 7 or Eq. 5 yields the most reliable results compared to experiment, and whether the inclusion of relativity can alter conclusions.

The first objective of this contribution is thus to shed light on the effect of relativity on Mössbauer isomer shifts of iron compounds using a hierarchy of relativistic Hamiltonians, comprising for example the four-component Dirac-Coulomb as well as the eXact two-Component (X2C)[27] Hamiltonian. To the best of our knowledge, this is the first time the X2C Hamiltonian and its spin-free variant are employed to calculate Mössbauer parameters of iron. It is also the first presentation

of four-component DFT and two-component CCSD(T) calculations of Mössbauer isomer shifts on larger inorganic molecules. Since two-component methods at the SCF level are by far compu-

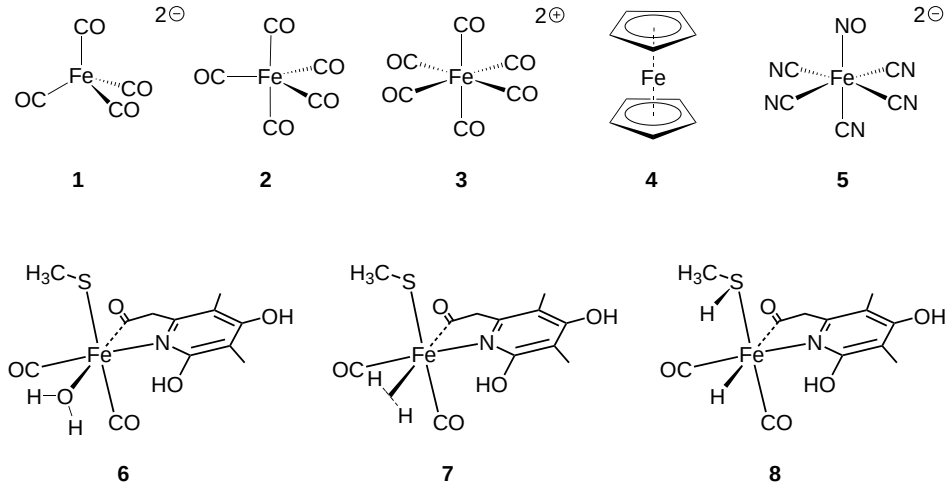

Figure 1: Structures used in this study. Molecules **1**–**5** are used for investigating the relativistic methods, while **6**–**8** are the target model structures for [Fe]-hydrogenase.

tationally less costly than four-component methods it will significantly broaden its applicability provided that similar accuracy can be reached within both approaches. All relativistic methods are compared to the non-relativistic Hamiltonian where both a finite sized and a point charge nuclei was employed. As a test set for the various relativistic models, we consider the closed-shell (low-spin) molecules **1**–**5**, displayed in Figure Figure 1.

The second objective of this study is to advertise the use of a genuine relativistic *ansatz* in computational bio-inorganic chemistry and the advantages that accrued by such an approach. To this end, we selected the recently characterized [Fe]-hydrogenase[28–30] which stands out from other classes of hydrogenases as it contains no iron-sulfur clusters as well as only a mono-nuclear metal site. Mössbauer studies on [Fe]-hydrogenase have been carried out by Shima et al.[31] In this paper we use the correlation plots from molecules **1**– **5** to calculate isomer shifts for the [Fe]-hydrogenase intermediates. These isomer shifts are then compared to the experimental data. It is noted that molecules **1**–**5** are well suited for this purpose, having the same spin states and similar ligands as the [Fe]-hydrogenase active site. To investigate whether the X2C is more generally applicable for iron compounds, we will in a follow-up study extend the set **1**– **5** to comprise also open-shell iron

complexes.

Despite having a somewhat simpler structure than the bi-metallic hydrogenase enzymes, the exact binding site of H_2 and the reaction mechanism of H_2 splitting is not known yet. Structure **6** (Figure Figure 1) is a model of the structurally characterized enzyme, while **7** and **8** are models of two intermediates, which were recently proposed to be involved in the mechanism of H_2 splitting.[32] We have computed the isomer shift of all three molecules, **6**–**8** where the respective geometries have been optimized by a QM/MM procedure including the full protein, surrounded by a water sphere of 60 Å from the protein center.

The paper is organized as follows: In the following two sections we give a short introduction to the theoretical framework applied in this contribution and provide computational details. Next we discuss our isomer shift data obtained at various level of theory and in comparison to experiment as well as the application of our final best model to the isomer shift determination of [Fe]-hydrogenase model systems. In the final section we draw conclusions and give an outlook to ongoing future work.

Theory

In this section we briefly introduce the relativistic Hamiltonians used in the Mössbauer isomer shift calculations. The most precise relativistic model presented in this work relies on the Dirac-Coulomb (DC) Hamiltonian

$$\hat{H} = \sum_i c(\boldsymbol{\alpha} \cdot \boldsymbol{p}_i) + \boldsymbol{\beta}' mc^2 + \sum_{i<j} \frac{1}{r_{ij}} + V_{NN} \tag{8}$$

where $\boldsymbol{\beta}' = \boldsymbol{\beta} - \boldsymbol{I}$ and $\boldsymbol{\alpha}$ and $\boldsymbol{\beta}$ are the 4x4 matrices

$$\boldsymbol{\beta} = \begin{pmatrix} \boldsymbol{I} & \boldsymbol{0} \\ \boldsymbol{0} & -\boldsymbol{I} \end{pmatrix} \qquad \boldsymbol{\alpha} = \begin{pmatrix} \boldsymbol{0} & \boldsymbol{\sigma}_i \\ \boldsymbol{\sigma}_i & \boldsymbol{0} \end{pmatrix} \tag{9}$$

$\boldsymbol{I}$ is the identity matrix and $\boldsymbol{\sigma}$ are the Pauli spin matrices. The DC Hamiltonian includes electron-electron repulsion through the instantaneous Coulomb interaction. This corresponds to the zeroth-order term of an expansion of the full relativistic two-electron interaction in orders of c^{-2}, which is sufficient for most chemical purposes.[33] Although the two-electron operator in the Dirac-Coulomb Hamiltonian has the same form as the non-relativistic electronic Hamiltonian, its physical content is different, for instance giving raise to spin-same orbit interaction.[34] There are several ways to transform the Hamiltonian in Eq. 8 to a two component Hamiltonian,[34] thereby reducing the complexity of the computational problem. One such Hamiltonian is based on the Zeroth Order Regular Approximation[35,36] (ZORA) and has been used extensively in Mössbauer studies. Filatov and coworkers have on the other hand introduced the use of the Normalized Elimination of the Small Component (NESC).[37] In the present work we investigate the use of the closely related eXact 2-Component (X2C) Hamiltonian, using the formalism of Ref. 27.

Results and discussion

In this section we compare first three different relativistic methods of increasing accuracy. We also comment on the use of CC data in iron Mössbauer spectroscopy, and relate the data obtained here to previous benchmark studies. Next, a method which employs fitting (Eq. 7) and a method that does not require fitting (Eq. 5) are compared to experiment with respect to their performance. The results from this calibration study is then used to investigate [Fe]-hydrogenase intermediates as displayed in Figure Figure 1.

Comparison of Relativistic Models and Methods

Calculated effective densities versus the experimental Mössbauer shifts are shown in Figure Figure 2 for the relativistic (left) and non-relativistic Hamiltonians (right). Both methods show a good linear correlation as could be expected. The fitting constants have been compiled in Table Table 1 (PBE functional) and Table 2 (PBE0 functional). All the used experimental data used for the fit-

ting have been compiled in Table 1 in the supplementary material and is given relative to iron foil (α-Fe). Starting with the relativistic methods at the right-hand side of Figure Figure 2, there is

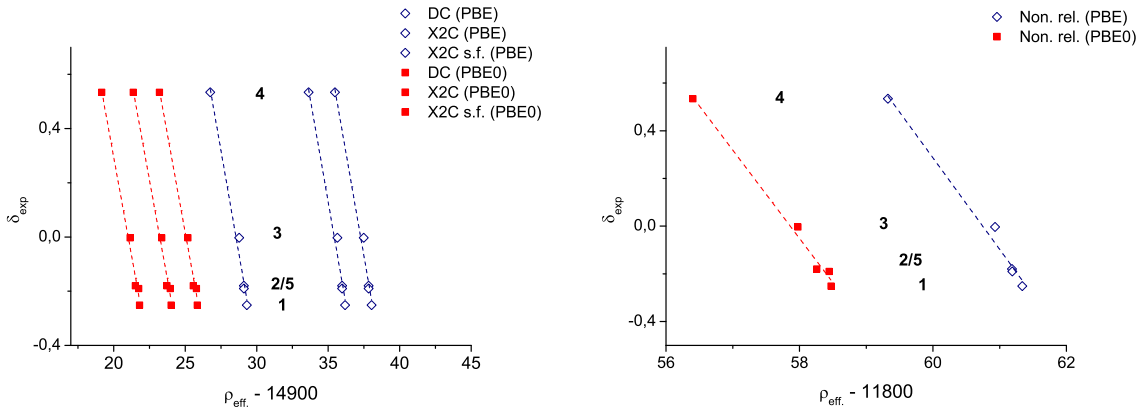

Figure 2: Correlation between effective densities on iron and experimental isomer shifts (Eq. 7). DC is the Dirac-Coulomb model, X2C is the eXact two-Component model and X2C(s.f.) refers to the X2C spin-free approach. The molecules **2** and **5** have almost identical effective densities in the relativistic models, whereas for the non-relativistic model the effective densities differ slightly.

some obvious difference in the absolute effective densities between the relativistic Hamiltonians. The trends, however, are identical, which is also reflected in the slopes of the linear correlation plots. In fact, the change between the PBE0 functional (with exact exchange) and the PBE functional is larger than the change within the relativistic level of approximation. A comparison

Table 1: Fitting parameters (Eq. 7) for the correlation plots in Figure Figure 2 with the PBE functional. In all cases C is kept fixed under the fit. Uncertainties are shown in parentheses.

Method	DC	X2C	X2C (s.f.)	Non-rel
a ($\mathrm{mm\,s^{-1}\,a_0^{-3}}$)	-0.303 (0.02)	-0.303 (0.02)	-0.303 (0.02)	-0.384 (0.0264)
b ($\mathrm{mm\,s^{-1}}$)	8.653 (0.570)	11.289 (0.743)	10.747 (0.707)	23.319 (1.607)
C (a_0^{-3})	14900	14900	14900	11800
R^2	0.9830	0.9830	0.9830	0.9813

between the X2C and its spin-free version reveals that spin-orbit effects are rather small for the iron compounds studied here although we are concerned with a property near the heavy iron nucleus. Taking into account scalar relativistic effects is on the other hand inevitable as can be seen from the large difference in both a and b parameters between the spin-free X2C model and the

Table 2: Fitting parameters (Eq. 7) for the correlation plots in Figure Figure 2 with the PBE0 functional. In all cases C is kept fixed under the fit. Uncertainties are shown in parentheses.

Method	DC	X2C	X2C (s.f.)	Non-rel
a ($\mathrm{mm\,s^{-1}\,a_0^{-3}}$)	-0.291 (0.015)	-0.291 (0.015)	-0.291 (0.015)	-0.370 (0.021)
b ($\mathrm{mm\,s^{-1}}$)	6.115 (0.317)	7.291 (0.378)	7.291 (0.378)	21.400 (1.209)
C (a_0^{-3})	14900	14900	14900	11800
R^2	0.9894	0.9894	0.9894	0.9874

non-relativistic calculations. Though the data are not shown here, contact densities were also calculated for both the PBE and PBE0 functionals and all relativistic models. The contact densities are generally slightly larger in absolute numbers than the effective densities, but give rise to very similar isomer shifts. Thus the effect of using contact rather than effective densities is small (this will be elaborated in the section concerned with the projection analysis below). Comparing contact densities between non-relativistic calculations with and without finite nucleus models, the effect of the finite nucleus treatment is found to be even negligible. However, it should be stressed that a finite nucleus treatment becomes mandatory in four- or two-component relativistic calculations due to weak singularities in the relativistic wave function at the origin of a point nucleus.

In order to have high-quality computational reference data, CC calculations were performed. As a by-product, it allowed us to investigate the effect of taking into account an increasing level of electron correlation, by comparing with Hartree-Fock (HF), second-order Møller-Plesset (MP2) and Coupled Cluster with Single and Doubles (CCSD). A subset of the CC results is listed in Table Table 3, while the complete set has been compiled in the supplementary material. An inspection

Table 3: Difference in contact densities ($\Delta\rho_0$) calculated with various methods. The $\Delta\rho_0$ values are reported w.r.t. $[Fe(NO)(CN)_5]^{2-}$ and are given in a_0^{-3}. All results are calculated with the spin-free X2C Hamiltonian.

Method	$\Delta\rho_0^{\mathrm{HF}}$	$\Delta\rho_0^{\mathrm{MP2}}$	$\Delta\rho_0^{\mathrm{CCSD}}$	$\Delta\rho_0^{\mathrm{PBE}}$	$\Delta\rho_0^{\mathrm{PBE0}}$
$Fe(CO)_4]^{2-}$	0.60	-1.87	0.05	0.21	0.06
$Fe(CO)_5$	-0.37	0.35	0.65	0.00	-0.23
$Fe(CO)_6]^{2+}$	-1.13	-0.82	-0.69	-0.33	-0.61

of Table Table 3 reveals that the trends in HF and the DFT functionals are similar (and correlate linearly with the experimental trend). Inclusion of dynamical correlation through MP2 leads to isomer shifts which are significantly off. Coupled Cluster with singles and doubles (CCSD) is again closer to the trend observed for HF, DFT and experiment, but $Fe(CO)_5$ is still an outlier. Perturbative inclusion of triples was also attempted, but did not yield a particular improvement. In fact, while the change for ρ_0^{CCSD} to $\rho_0^{\mathrm{CCSD(T)}}$ in molecules **1**–**3** was rather moderate, the change for $[Fe(NO)(CN)_5]^{2-}$ (**5**) was surprisingly high (see Table S4 in the supplementary material), leading to very large shifts (since **5** was used as reference). The trends for CCSD(T) and CCSD are however, similar. Thus, with the exclusion of $Fe(CO)_5$, PBE0 and CCSD provide very similar shifts in contact density, but both the small size of the test set and the spurious large change in contact density upon inclusion of the (perturbative) triples correction for $[Fe(NO)(CN)_5]^{2-}$, render the current conclusion very tentative with respect to a comparison of the CC results with DFT results. The fact that perturbative treatments are seen to be problematic, along with rather high T_1 amplitudes, indicate large orbital relaxation effects and/or a potential multiconfigurational ground state wave function. Thus, it is likely that at least a full inclusion of triples and possibly quadruples or a inherently multiconfigurational treatment, for example CASSCF followed by multireference CC or CI, is necessary to obtain reliable high-quality results. The former is possible in `Dirac` as such through the interface[56] to the MRCC program of M. Kállay[57,58] but demands at present computational resources beyond our capabilities.

Some of the molecules from our test set have also been used by others to validate computed isomer shifts. Relativistic calculations were carried out by Kurian and Filatov[20,22] for the molecules **2** and **4** using the spin-free Normalized Elimination of Small Component (NESC) Hamiltonian approach. Apart from the varying relativistic models, a direct comparison with the studies by Kurian and Filatov is not feasible since slightly different molecular geometries have been used and results are often reported in a different manner, either in total densities or in isomer shifts with respect to a reference (Eq. 5 with α from ref. 20). After correcting for the reference compounds, the relative values between $[Fe(CO)_4]^{2-}$ and $Fe(CO)_5$ are in reasonable agreement: We obtain 0.147 versus

0.16 in ref. 20. In addition, we find a reasonable agreement between our and the total density of $Fe(Cp)_2$ as reported in Ref. 22. Although we use an inherently relativistic approach, it seems nevertheless worthwhile to compare to the fits obtained by using non-relativistic B2-PLYP densities, scaled with $\bar{\rho}_{\text{rel}}/\bar{\rho}_{\text{non-rel}}$ from atomic CCSD(T) calculations.[22] This approach yields a correlation constant of $a = -0.306 a_0^{-3}$ mm s^{-1} and compares quite well with our value from fully relativistic calculations at the DFT/PBE level. The correlation constant obtained at the DFT/PBE0 level is (in absolute numbers) slightly lower, but still in reasonable agreement.

Comparison to Experiment

In Tables Table 4 and Table 5 the calculated isomer shift are compared to experiment, by using either Eq. 7 and the appropriate fitting constants (Tables Table 1 and Table 2) or Eq. 5 with $[Fe(NO)(CN)_5]^{2-}$ as reference. In the case of fitting, good results can be obtained both with and without relativistic effects. This is mainly caused by the large difference in linear correlation constants, a between non-relativistic and relativistic methods. Thus, the non-relativistic methods are indirectly corrected through a. Since the linear correlation constant a with all relativistic methods is rather close to the experimentally obtained α,[21] the best result is indeed obtained with an inclusion of relativistic effects even for the first-row transition metal iron. In conclusion, both relativistic and non-relativistic methods can be used to estimate shifts for iron Mössbauer spectroscopy. However, the most coherent and transparent results are obtained using relativistic methods, leading to similar results for approaches which employ fitting procedures and those based on the use of a reference compound.

A note concerning $Fe(CO)_5$ should be made. As pointed out in a previous study on isomer shifts,[63] this compound has been measured quite often where a wide spread of experimental isomer shifts has been obtained ranging from 0.00 to -0.18. From the linear correlation plot displayed in Figure 2 it is obvious that a value closer to -0.18 will lead to a linear relationship between the effective density and the isomer shift.

We conclude this paragraph by commenting on the performance of the different DFT exchange-

Table 4: Calculated and experimental isomer shifts ($mm\,s^{-1}$) for the molecules **1**–**5**. The calculation of isomer shifts are performed with the Dirac-Coulomb (DC), eXact two-Component (X2C) or the spin-free (s.f.) X2C Hamiltonians, using either Eqs. 7 or 5. Experimental values have been extracted from Refs.[59–63] The different experimental values are due to difference in reference compounds.

Fit[a] (PBE)	$[Fe(CO)_4]^{2-}$	$Fe(CO)_5$	$[Fe(CO)_6]^{2+}$	$Fe(Cp)_2$	$[Fe(NO)(CN)_5]^{2-}$
DC	-0.231	-0.168	-0.068	0.545	-0.168
X2C	-0.231	-0.168	-0.066	0.545	-0.168
X2C (s.f.)	-0.231	-0.168	-0.066	0.545	-0.168
Non-rel	-0.227	-0.168	-0.071	0.545	-0.170
Exp.	-0.251	-0.18	-0.003	0.534	-0.19
No Fit[b] (PBE)					
4C	-0.064	0.000	0.103	0.729	0.000
X2C	-0.064	0.000	0.103	0.730	0.000
X2C (s.f.)	-0.064	0.000	0.103	0.729	0.000
Non-rel	-0.046	0.002	0.080	0.578	0.000
Exp.	-0.061	0.010	0.187	0.724	0.000

[a] The isomer shift is calculated with Eq. 7 using the parameters from Table 1. The experimental values refer to iron foil (α-Fe).

[b] The isomer shift is calculated from Eq. 5 with $\alpha = -0.31\ a_0^3$ mm s^{-1} using $[Fe(NO)(CN)_5]^{2-}$ as reference.

correlation functionals. This issue has been widely discussed for isomer shifts and it seems to be a common conclusion that functionals with a high amount of exact exchange are to be preferred.[10,20] Yet, using the X2C Hamiltonian and for the molecules investigated here, we find the the PBE functional performs well and is not inferior to the hybrid version PBE0 – the latter having a high amount of exact exchange (25%). Although our present CCSD results indicate that PBE0 is more accurate, a test with a larger and more varied test set should be performed before reaching a final conclusion regarding the best suited DFT functional for the X2C Hamiltonian. This caution seems to be in order since the current CC results furthermore suggest that higher order excitation ranks in the coupled cluster expansions might be required.

Table 5: Calculated and experimental isomer shifts ($mm\,s^{-1}$) for molecules **1**–**5**. The calculation of isomer shifts are performed with the Dirac-Coulomb (DC), eXact two-Component (X2C) or the spin-free X2C Hamiltonians, using either Eqs. 7 or 5. Experimental values have been extracted from refs. 59–63. The different experimental values are due to difference in reference compounds.

Fit[a] (PBE0)	$[Fe(CO)_4]^{2-}$	$Fe(CO)_5$	$[Fe(CO)_6]^{2+}$	$Fe(Cp)_2$	$[Fe(NO)(CN)_5]^{2-}$
4C	-0.231	-0.148	-0.038	0.540	-0.212
X2C	-0.230	-0.148	-0.038	0.540	-0.212
X2C (s.f.)	-0.230	-0.147	-0.038	0.540	-0.212
Non-rel	-0.226	-0.147	-0.042	0.540	-0.215
Exp.	-0.251	-0.18	-0.003	0.534	-0.19
No Fit[b] (PBE0)					
4C	-0.018	0.071	0.189	0.813	0.000
X2C	-0.018	0.071	0.189	0.813	0.000
X2C (s.f.)	-0.018	0.071	0.189	0.812	0.000
Non-rel	-0.009	0.058	0.146	0.634	0.000
Exp.	-0.061	0.010	0.187	0.724	0.000

[a] The isomer shift is calculated with Eq. 7 using the parameters from Table Table 2. The experimental values refer to iron foil (α-Fe).

[b] The isomer shift is calculated from Eq. 5 with $\alpha = -0.31$ using $[Fe(NO)(CN)_5]^{2-}$ as reference

Hydrogenase Intermediates

Isomer shifts

Encouraged by the results from the previous subsection, we have applied the X2C/DFT model to a biologically relevant iron system, namely the [Fe]-hydrogenase active site. The [Fe]-hydrogenase protein is found in certain methanogenic archaea and catalyzes the oxidation of H_2 in an intermediate step of the reduction of CO_2 to methane. H_2 is presumably split by coordination to iron and a hydride abstracted by N^5,N^{10}-methenyl-tetrahydromethanopterin (methenyl-H_4MPT$^+$), but the detailed mechanism is still under debate.[30] A crystal structure of [Fe]-hydrogenase was reported by Shima *et al.*,[29] but the iron ligation was later reinterpreted following a X-ray crystallographic study of a mutated protein.[28] Shima and co-workers also carried out a Mössbauer study of the

full protein finding that the isomer shift did not change upon addition of H_2.[31] In the proposed catalytic mechanism, hydrogen activation is initiated by the H_2O/H_2 exchange in **6** to form **7** (see Figure Figure 1). In a computational study Yang and Hall found that the free energy barrier of H_2 cleavage in **7** to form the thermodynamically more stable **8** (-3.4 kcal/mol) was quite low (6.6 kcal/mol) and therefore suggested **8** as the resting state observed in the Mössbauer experiment. They further argued that the isomer shifts of **7** and **8** would be quite similar since the Mulliken charges of iron in the two species are quite close (+0.142 and +0.138). We have, however, calculated the isomer shifts of all three species, as shown in Table Table 6 . As can be seen from our results the isomer shift of **8** is appreciable different from the predicted isomer shift of **6** and **7**. An indirect estimate of Mössbauer isomer shifts based on Mulliken charges can accordingly not be recommended. The isomer shifts of **6** and **7** are on the other hand quite close to the experimental value, in particular when taking into account that the typical experimental error is $\pm$ 0.01 $\mathrm{mm\,s^{-1}}$.[31] Hence, according to our present results it seems likely that an intermediate of the

Table 6: Isomer shifts ($\mathrm{mm\,s^{-1}}$) calculated for molecules **6**–**8** with the X2C Hamiltonian and the PBE0 functional, using either Eqs. 7 or 5. A single experimental value is given since the Mössbauer isomer shift did not change upon addition of H_2.[31] Note that for the intermediate **8**, the $^{\ominus}SCH_3$ group is altered to a protonated $HSCH_3$ group (see Figure Figure 1).

$[Fe(L)(pyridone)(CO)_2(SCH_3)]^+$	L = H_2O (**6**)	L = H_2 (**7**)	L = $H^{\ominus}$ (**8**)	Exp.
Isomer shift[a]	0.045	0.034	-0.105	0.060
Isomer shift[b]	0.275	0.264	0.114	0.250

[a] The isomer shift is calculated from Eq. 7 using the parameters from Table 2. The experimental values refer to iron foil (α-Fe).

[b] The isomer shift is calculated from Eq. 5 with $\alpha = -0.31$ using $[Fe(NO)(CN)_5]^{2-}$ as reference.

type **7** would go unnoticed in a Mössbauer study. On the other hand, the hydride intermediate **8** has a calculated isomer shift which is significant off the experimental shift, and quite different from both **6** and **7**. This observation leads us to conclude that **8** does not build up in significant concentrations during the Mössbauer experiment, although **8** could still be involved in the catalytic cycle. In addition, it should be emphasized that the current studies are performed without taking

into account the (methenyl-H_4MPT^+) substrate, which, according to ref. 31, is supposed to have a minor effect on the isomer shift only (suggesting rather small changes in the iron coordination sphere). To shed further light on the latter issue we are pursuing at present QM/MM optimizations of **6**–**8** that include the substrate.

Projection analysis

The difference of 0.139 $mm\,s^{-1}$ in calculated isomer shifts of molecules **7** and **8** shown in Table Table 6 translates into a 41 ppm change of contact density, a change whose origin is quite subtle. Detailed analysis[25] shows that in a relativistic framework the contact density ρ_0 has contributions from atomic $s_{1/2}$ and $p_{1/2}$ orbitals only, from the large and small components, respectively. These contributions are compiled in Table Table 7 for the neutral iron atom. The table also illustrates that the contact density as expected overestimates the effective density $\bar{\rho}_e$, yet for the iron atom constitutes a good approximation to it, since the error is on the order of merely 1 % . Comparison between calculated effective and contact densities for molecules **1**–**8** furthermore shows that this 1% error is quite systematic in nature. On the other hand, the effective density can be calculated at the same computational cost and is therefore recommended.

Table 7: Orbital contributions (in a_0^{-3}) to the contact density ρ_0 and effective density $\bar{\rho}_e$ of the iron atom in its ground state electron configuration $[Ar]3d^6 4s^2$ obtained with the PBE0 functional and the X2C Hamiltonian. Negligible contributions to $\bar{\rho}_e$ from the $np_{3/2}$ and $3d_{3/2,5/2}$ orbitals have been omitted from the table.

Orbital	ρ_0	$\bar{\rho}_e$
$1s_{1/2}$	13642.75	13463.36
$2s_{1/2}$	1283.89	1266.99
$3s_{1/2}$	184.07	181.64
$4s_{1/2}$	11.16	11.01
$2p_{1/2}$	6.16	6.16
$2p_{1/2}$	0.85	0.85
Total	15128.87	14930.02

We have tried to rationalize the variations in isomer shifts of the model structures for [Fe]-

hydrogenase by means of projection analysis.[64,65] The projection analysis is based on the expansion of molecular orbitals $\{\psi_k^{\mathrm{MO}}\}$ into a set of pre-calculated atomic orbitals $\{\psi_i^{\mathrm{A}}\}$

$$\psi_k^{\mathrm{MO}} = \sum_A \sum_{i \in A} \psi_i^{\mathrm{A}} c_{ik}^{\mathrm{A}} + \psi_k^{\mathrm{pol}} \tag{10}$$

where the orthogonal complement ψ_k^{pol} is denoted the polarization contribution and should in general be small for a meaningful analysis. Insertion into the expression of the expectation value of an operator $\hat{\Omega}$ at the SCF-level

$$\langle \Omega \rangle = \sum_k^{occ} \langle\, \psi_k \,|\, \hat{\Omega} \,|\, \psi_k \,\rangle = \sum_A \sum_{i \in A} \sum_B \sum_{j \in B} \langle\, \psi_i^{\mathrm{A}} \,|\, \hat{\Omega} \,|\, \psi_j^{\mathrm{B}} \,\rangle D_{ji}^{BA} + \langle\, \mathrm{pol} \,\rangle; \quad D_{ji}^{BA} = \sum_k^{occ} c_{ik}^{\mathrm{A}*} c_{jk}^{\mathrm{B}} \tag{11}$$

allows the distinction of *intra-atomic* ($A = B$) and *inter-atomic* ($A \neq B$) contributions. Setting the above operator $\hat{\Omega} = 1$ we can carry out a population analysis similar to the Mulliken one, but without the strong basis set dependence.[64] For the present analysis we calculated the atoms in their electronic ground state configuration using fractional occupation and employed all occupied orbitals of the atoms, adding a second *s* orbital for the hydrogens as well as the 4*p* orbitals of iron. This set of atomic orbitals does not span the molecular orbitals fully. The polarization contribution amounts to about one electron, which is a bit high, but constant for all three molecules and has negligible contribution to the contact and effective densities. We therefore believe that the projection analysis is reliable for these systems.

Table 8: Electron configuration and charge of iron in molecules **6** – **8** from projection analysis.

	3d	4s	4p	Q^{Fe}
6	6.74	0.20	0.21	+0.86
7	6.79	0.26	0.24	+0.70
8	6.77	0.27	0.27	+0.69

In Table Table 8 we give the electron configuration and charge of iron in molecules **6**–**8** obtained from gross populations. The calculated charges *Q* for molecules **7** and **8** are indeed quite similar, but somewhat larger than the Mulliken charges reported by Yang and Hall,[32] and con-

sistent with a Fe^{II} rather than Fe^{0} oxidation state. As already stated above, the charges do not correlate well with a calculated isomer shifts reported in Table Table 6. We also note that the 3*d* populations of **7** and **8** are basically identical, and so the difference in isomer shifts can not be attributed to a screening mechanism whereby increased 3*d* population implies increased screening and thereby reduced contact density of the 3*s* orbitals in particular.[9,14]

Table 9: Projection analysis of Fe contact density (in a_0^{-3}), relative to the ground state atom, at the X2C/PBE0 level.

		6	**7**	**8**
Fe (intra)		-4.15	-4.08	-3.54
pm ($i = j$)		4.02	3.20	3.83
	$1s_{1/2}$	0.59	0.55	0.58
	$2s_{1/2}$	2.98	2.75	2.90
	$2p_{1/2}$	0.00	0.00	0.00
	$3s_{1/2}$	10.81	10.07	10.64
	$3p_{1/2}$	0.01	0.01	0.02
	$4s_{1/2}$	-10.39	-10.18	-10.30
hyb ($i \neq j$)		-8.17	-7.29	-7.36
Interatomic contribution		-0.37	-0.35	-0.38
Polarization contribution		-0.68	-0.71	-0.75
Total		–5.18	-5.15	-4.66

We therefore turn to projection analysis, compiled in Table Table 9, which shows that the Fe contact density for all three species is, as expected, dominated by intra-atomic contributions from the iron center itself. The intra-atomic contributions further split into diagonal ($j = i$) and hybridization ($j \neq i$) contributions, cf. Eq. (11), where the latter contributions arise from the breakdown of atomic symmetry in the molecule. Hybridization contributions involving the same atomic types, e.g. $s_{1/2}$, may also be associated with a radial re-polarization of atomic orbitals within the molecule. From Table Table 9 it is seen that the hybridization contributions to **7** and **8** are quite similar and distinct from those of **6**. The major difference between molecules **7** and **8** originates from the diagonal contribution involving the Fe $3s_{1/2}$ orbitals. The value of the diagonal density matrix element $D^{Fe,Fe}_{3s,3s}$ is 2.1175, 2.1094 and 2.1156 for molecules **6**, **7** and **8**, respectively,

compared to rigorously 2.0000 for the neutral iron atom. The differences are very small, but become crucial when multiplied with the atomic matrix element (92.03 a_0^{-3}) in Eq. 11. Values larger than two of the diagonal density matrix element arises from overlap of the iron $3s_{1/2}$ orbital with ligand orbitals. In molecule **8** we find for instance overlap on the order of 0.13 between 3*s* and the hydride coordinated to iron. In summary, our analysis shows that the small, but significant difference in isomer shifts between molecules **7** and **8** arises as the result of overlap between iron core orbitals and ligand orbitals. Such an overlap effect has been discussed previously[66–69] , but in the context of molecular wave functions assembled from pre-calculated atomic orbitals and where iron orbitals where projected out from ligand ones for orthonormality. This can be contrasted with the present approach in which fully relaxed molecular orbitals are expanded in pre-calculated atomic ones.

Conclusion

We have investigated relativistic Hamiltonians of increasing sophistication for isomer shift on iron compounds. The set of chosen Hamiltonians comprises the four-component Dirac-Coulomb and the two-component X2C Hamiltonians with or without spin-orbit coupling. In addition, all relativistic data has been compared to results obtained with the common non-relativistic Schrödinger Hamiltonian. Similar accuracy is achieved for both the full four-component reference Hamiltonian as well as the X2C Hamiltonian, though the latter is computationally less expensive. Further computational savings are possible since spin-orbit coupling can also safely be neglected. Linear correlation plots using effective densities versus experimental isomer shift yield a slope of $a = -0.303\ a_0^3$ mm s^{-1} (PBE functional) which is in close agreement with experimental findings ($\alpha = -0.31\ a_0^3$ mm s^{-1}). Using this correlation constant isomer shifts of very similar quality can be obtained both with and without fitting. On the contrary, the non-relativistic calculations give a significantly different slope and the good correspondence is eventually lost between both approaches.

Using either method — with and without fitting –, the X2C/DFT model is applied to three forms of [Fe]-hydrogenase, which have been proposed to be involved in its catalytic cycle of H_2 cleavage. For these systems we find that both a form without H_2 (**6**) and the intermediate with H_2 bound side-on to the Fe center (**7**) have similar isomer shifts which are in good agreement with the experimental value. Thus, our theoretical results suggest that a Mössbauer study cannot be used to discriminate between these two states. The third discussed state – the hydride intermediate **8** – has a calculated isomer shift that does not only differ significantly from the experimental shift but also from those of **6** and **7**. These findings prompt the conclusion that **8** does not build up in significant concentrations during the Mössbauer experiment. Projection analysis of the associated contact density of the molecules **6-8** reveals that the difference in isomer shift between intermediates **7** and **8** arises primarily from small, but non-negligible overlap between the iron 3*s* orbital and ligand orbitals, in particular the 1*s* orbital of the hydride coordinated to iron in **8**.

In this work our primary focus has been on closed shell and low-spin iron complexes, respectively. Although we expect that our present conclusions will hold also in the more general case of open-shell/high-spin iron complexes we will discuss these issues in a forthcoming publication using a genuine, relativistic open-shell two- and four-component self-consistent-field approach.

Computational Details

The applied test set comprises the molecules **1**–**5** displayed in Figure Figure 1. The structures **1**–**5** were optimized with the Gaussian09 program[38] using the BP86 functional[39,40] and a TZVP basis.[41,42] The experimental isomer shifts used as reference data in this study are provided in Table 1 in the supplementary material. The models for the [Fe]-hydrogenase intermediates **6**–**8** (see Figure Figure 1) have been obtained and optimized with DFT, considering the immediate coordination geometry of the iron as the QM region and including a full protein matrix. The optimization was performed using the QM/MM procedure defined by the ComQum program which has been developed by Ryde and coworkers.[43,44] From the fully optimized structures the active site model

was cut out as shown in Figure Figure 1. Details concerning these optimizations will be published elsewhere. All relativistic calculations were performed with an development version of the `Dirac` program package.[45] For the molecules **1**–**5**, calculations were performed with the Dirac Coulomb Hamiltonian including all integral classes arising from the two-electron Coulomb term (keyword `.DOSSSS`). The next level of approximation was to use the eXact 2-component Hamiltonian,[27] both a spin-free and a spin-orbit variant, where the spin-same orbit contributions obtained by an atomic mean-field integral (AMFI) approximation.[46,47] In case of the [Fe]-hydrogenase intermediates **6**–**8** the latter relativistic Hamiltonian model was exclusively applied. SCF calculations for the molecules **1**–**5** were performed at the Hartree-Fock and DFT level of theory, respectively. For the latter, several exchange-correlation functionals were chosen, namely LDA (VWN5)[48] (not shown), PBE[49] and PBE0.[50] The [Fe]-hydrogenase intermediates **6**–**8** were calculated with PBE0 only. For the ligands we used a Dunning cc-pVTZ basis set[51] and for the iron core a triple-ζ Dyall basis set[52] augmented with one steep s-function ($\xi = 3.02252694 \cdot 10^8$) and one steep p function ($\xi = 1.83449497 \cdot 10^5$). All basis sets in the above calculations were kept in their uncontracted form, which is necessary in the current implementation of the AMFI approximation. Although this constraint is not necessary for the spin free X2C model, we chose to keep the basis sets uncontracted to facilitate a direct comparison between the methods. Coupled Cluster (CC) calculations have been performed for molecules **1**–**3** and **5**. The ferrocene complex (**4**) is computationally quite demanding and has not been run with CC methods. Following the typical protocol in experimental studies, we used **5** as reference in the CC calculations. The calculations were performed with the Relativistic Coupled Cluster program (RELCCSD) implemented in `Dirac`.[53–55] Contact densities were calculated based on the prescription by Knecht et al.[25] for mercury compounds. Accordingly, the correlation contribution $\rho_0^{\text{corr.}}$ is calculated from finite-field calculations which is then added to the analytical HF value, ρ_0^{HF}. We will use ρ_0^{MP2}, ρ_0^{CCSD} and $\rho_0^{\text{CCSD(T)}}$ to denote the sum of ρ_0^{HF} and ρ_0^{corr} for the given correlated method. A careful investigation was performed to find the optimal stencil expression and field strength for the finite-field calculations (see supplementary material). All MP2 and CC results reported here are from 5-point stencils, using a field strength of $h = 10^{-7}$

a.u. In order to keep the extra cost for the CC calculations minimal compared to DFT, all of the former were performed with the spin-free X2C method and ligand atom basis sets were contracted. Comparison between ρ_0^{HF} with- and without contracted ligand basis functions shows that this has only negligible influence of the isomer shifts. Furthermore, core orbitals and very diffuse, virtual orbitals were kept frozen. The occupied active space in the CC calculations was chosen to comprise in each case the $(n-1)$sp $n$sp shell of the ligand atoms (outer core and valence shells) as well as the $(n-1)$spd ns shell of iron. The high cutoff in the active virtual space at typically 15 -16 eV, and on one occasion (**3**) even much higher, important core-valence correlating functions were taken into account.

Acknowledgement

E.D.H thanks the OTICON and Augustinus foundations for stipends. S. K. gratefully acknowledges a postdoctoral research grant from the Natural Science Foundation (FNU) of the Danish Agency for Science, Technology and Innovation (grant number: 10-082944) during his postdoctoral stay at SDU Odense. The authors thank the Danish Center for Scientific Computing (DCSC) for computational resources.

Supporting Information Available

References

(1)

(2) Fontecilla-Camps, J. C.; Volbeda, A.; Cavazza, C.; Nicolet, Y. *Chem. Rev.* **2007**, *107*, 4273–4303.

(3) Lubitz, W.; Reijerse, E.; van Gastel, M. *Chem. Rev.* **2007**, *107*, 4331–4365.

(4) Mössbauer, R. L. *Z. Phys.* **1958**, *151*, 124–143.

(5) Gütlich, P.; Schröder, C. *Bunsenmagazin* **2010**, *12*, 4–22.

(6) Gütlich, P.; Bill, E.; Trautwein, A. X. In *Mössbauer Spectroscopy and Transition Metal Chemistry. Fundamentals and Applications*; Gütlich, P.; Bill, E.; Trautwein, A. X., Eds.; Springer, 2011, pp 25–71.

(7) Melissinos, A. C.; Davis, S. P. *Phys. Rev.* **1959**, *115*, 130–137.

(8) Kistner, O. C.; Sunyar, A. W. *Phys. Rev. Lett.* **1960**, *4*, 412–415.

(9) Walker, L. R.; Wertheim, G. K.; Jaccarino, V. *Phys. Rev. Lett.* **1961**, *6*, 98–101.

(10) Filatov, M. *Coord. Chem. Rev.* **2009**, *253*, 594–605.

(11) Duff, K. J. *Phys. Rev. B* **1974**, *9*, 66–72.

(12) Trautwein, A.; Harris, F. E.; Freeman, A. J.; Desclaux, J. P. *Phys. Rev. B* **1975**, 4101–4105.

(13) Nieuwpoort, W. C.; Post, D.; van Duijnen, P. T. *Phys. Rev. B* **1978**, *17*, 91–98.

(14) Neese, F. *Inorg. Chim. Acta* **2002**, *337*, 181–192.

(15) Reschke, A.; Trautwein, A.; Desclaux, J. P. *J. Phys. Chem. Solids* **1977**, *38*, 837–841.

(16) Zhang, Y.; Mao, J.; Oldfield, E. *J. Am. Chem. Soc.* **2002**, *124*, 7829–7839.

(17) Li, M.; Bonnet, D.; Bill, E.; Neese, F.; Weyhermüller, T.; Blum, N.; Sellmann, D.; Wieghardt, K. *Inorg. Chem.* **2002**, *41*, 3444–3456.

(18) Zhang, Y.; Oldfield, E. *J. Am. Chem. Soc.* **2004**, *126*, 4470–4471.

(19) Filatov, M. *J. Chem. Phys.* **2007**, *127*, 084101.

(20) Kurian, R.; Filatov, M. *J. Chem. Theory Comput.* **2008**, *4*, 278–285.

(21) Ladrière, J.; Meykens, A.; Coussement, R.; Cogneau, M.; Boge, M.; Auric, P.; Bouchez, R.; Banabed, A.; Godard, J. *J. Phys. Coll. C2* **1979**, *40*, 20–22.

(22) Kurian, R.; Filatov, M. *Phys. Chem. Chem. Phys.* **2010**, *12*, 2758–2762.

(23) Sinnecker, S.; Slep, L. D.; Bill, E.; Neese, F. *Inorg. Chem.* **2005**, *44*, 2245–2254.

(24) Römelt, M.; Ye, S.; Neese, F. *Inorg. Chem.* **2009**, *48*, 784–785.

(25) Knecht, S.; Fux, S.; van Meer, R.; Visscher, L.; Reiher, M.; Saue, T. *Theo. Chem. Acc.* **2011**, *129*, 631–650.

(26) Fricke, B.; Waber, J. T. *Phys. Rev. B* **1972**, *5*, 3445.

(27) Iliaš, M.; Saue, T. *J. Chem. Phys.* **2007**, *126*, 064102.

(28) Hiromoto, T.; Ataka, K.; Pilak, O.; Vogt, S.; Stagni, M. S.; Meyer-Klaucke, W.; Warkentin, E.; Thauer, R. K.; Shima, S.; Ermler, U. *FEBS Lett.* **2009**, *583*, 585–590.

(29) Shima, S.; Pilak, O. abnd Vogt, S.; Schick, M.; Stagni, M. S.; Meyer-Klaucke, W.; Warkentin, E.; Thauer, R. K.; Ermler, U. *Science* **2008**, *321*, 572–575.

(30) Shima, S.; Ermler, U. *Eur. J. Inorg. Chem.* **2011**, 963–972.

(31) Shima, S.; Lyon, E. J.; Thauer, R. K.; Mienert, B.; Bill, E. *J. Am. Chem. Soc.* **2005**, *127*, 10430–10435.

(32) Yang, X.; Hall, M. B. *J. Am. Chem. Soc.* **2009**, *131*, 10901–10908.

(33) Visser, O.; Visscher, L.; Aerts, P. J. C.; Nieuwpoort, W. C. *Theo. Chem. Acc.* **1992**, *81*, 405–416.

(34) Saue, T. *ChemPhysChem* **2011**, *12*, 3077–3094.

(35) van Lenthe, E.; Baerends, E. J.; Snijders, J. G. *J. Chem. Phys.* **1993**, *99*, 4597–4610.

(36) Chang, C.; Pelissier, M.; Durand, P. *Phys. Scr.* **1986**, *34*, 394–404.

(37) Dyall, K. G. *J. Chem. Phys.* **1997**, *106*, 9618–9626.

(38) Frisch, M. J. et al. *Gaussian 09 Revision A.1*, 2009, Gaussian Inc. Wallingford CT 2009.

(39) Becke, A. D. *Phys. Rev. A* **1988**, *38*, 3098.

(40) Perdew, J. P. *Phys. Rev. B* **1986**, *33*, 8822.

(41) Schäfer, A.; Horn, H.; Ahlrichs, R. *J. Chem. Phys.* **1992**, *97*, 2571.

(42) Schäfer, A.; Huber, C.; Ahlrichs, R. *J. Chem. Phys.* **1994**, *100*, 5829.

(43) Ryde, U.; Olsson, M. H. M. *Int. J. Quant. Chem.* **2001**, *81*, 335–347.

(44) Ryde, U.; Olsen, L.; Nilson, K. *J. Comput. Chem.* **2002**, *23*, 1058–1070.

(45) DIRAC, a relativistic ab initio electronic structure program, Release DIRAC12 (2012), written by H. J. Aa. Jensen, R. Bast, T. Saue, and L. Visscher, with contributions from V. Bakken, K. G. Dyall, S. Dubillard, U. Ekström, E. Eliav, T. Enevoldsen, T. Fleig, O. Fossgaard, A. S. P. Gomes, T. Helgaker, J. K. Lærdahl, Y. S. Lee, J. Henriksson, M. Iliaš, Ch. R. Jacob, S. Knecht, S. Komorovský, O. Kullie, C. V. Larsen, H. S. Nataraj, P. Norman, G. Olejniczak, J. Olsen, Y. C. Park, J. K. Pedersen, M. Pernpointner, K. Ruud, P. Sałek, B. Schimmelpfennig, J. Sikkema, A. J. Thorvaldsen, J. Thyssen, J. van Stralen, S. Villaume, O. Visser, T. Winther, and S. Yamamoto (see http://www.diracprogram.org).

(46) Hess, B. A.; Marian, C. M.; Wahlgren, U.; Gropen, O. *Chem. Phys. Lett.* **1996**, *251*, 365–371.

(47) AMFI*: An Atomic Mean-Field Code*, B. Schimmelpfennig, Stockholm, Sweden, 1996.

(48) Vosko, S. H.; Wilk, L.; Nusair, M. *Can. J. Phys.* **1980**, *58*, 1200–1211.

(49) Perdew, J. P.; Burke, K.; Ernzerhof, M. *Phys. Rev. Lett.* **1996**, *77*, 3865–3868.

(50) Perdew, J. P.; Ernzerhof, M.; Burke, K. *J. Chem. Phys.* **1996**, *105*, 9982–9985.

(51) Dunning Jr., T. H. *J. Chem. Phys.* **1989**, *90*, 1007–1023.

(52) K. G. Dyall, private communication (2012).

(53) Visscher, L.; Lee, T. J.; Dyall, K. G. *J. Chem. Phys.* **1996**, *105*, 8769–8776.

(54) Visscher, L.; Eliav, E.; Kaldor, U. *J. Chem. Phys.* **2001**, *115*, 9720–9726.

(55) Pernpointner, M.; Visscher, L. *J. Comput. Chem.* **2003**, *24*, 754–759.

(56) Nataraj, H. S.; Kállay, M.; Visscher, L. *J. Chem. Phys.* **2010**, *133*, 234109.

(57) Kállay, M.; Surján, P. R. *J. Chem. Phys.* **2001**, *115*, 2945.

(58) MRCC, a string-based quantum chemical program suite written by M. Kállay. See also Ref. 57 as well as http://www.mrcc.hu/.

(59) Erickson, N. E.; Fairhall, A. W. *Inorg. Chem.* **1965**, *4*, 1320–1322.

(60) Kerler, W.; Neuwirth, W.; Fluck, E. *Z. Phys.* **1963**, *175*, 200–220.

(61) Bernhardt, E.; Bley, B.; Wartchow, R.; Willner, H.; Bill, E.; Kuhn, P.; Sham, I. H. T.; Bodenbinder, M.; Bröchler, R.; Aubke, F. *J. Am. Chem. Soc.* **1999**, *121*, 7188–7200.

(62) Lesikar, A. V. *J. Chem. Phys.* **1964**, *40*, 2746–2747.

(63) Nemykin, V. N.; Hadt, R. G. *Inorg. Chem.* **2006**, *45*, 8297–8307.

(64) Dubillard, S.; Rota, J.-B.; Saue, T.; Fægri, K. *J. Chem. Phys.* **2007**, *124*, 154307.

(65) Bast, R.; Koers, A.; Gomes, A. S. P.; Iliaš, M.; Visscher, L.; Schwerdtfeger, P.; Saue, T. *Phys. Chem. Chem. Phys.* **2010**, *13*, 854.

(66) Flygare, W. H.; Hafemeister, D. W. *J. Chem. Phys.* **1965**, *43*, 789–794.

(67) Šimánek, E.; Šroubek, Z. *Phys. Rev.* **1967**, *163*, 275–279.

(68) Walch, P. F.; Ellis, D. E. *Phys. Rev. B* **1973**, *7*, 903–907.

(69) Trautwein, A.; Harris, F. E. *Theor.Chim. Acta* **1973**, *30*, 45–58.

This material is available free of charge via the Internet at `http://pubs.acs.org`.